Study of vulnerable zones to soil instability by radar remote sensing, case of the Temsamane region in north Morocco

Mohammed Mourjane [1,*], *Naoual* El Hammouch [1], *Fatima* El Hammichi [1], *Mohammed* Benabdelhadi [2], *Hassan* Tabyaoui [1] *and Abderrahim* Lahrach [2]

[1]Naturals Resources and Environment Laboratory, Polydisciplinary Faculty of Taza, Sidi Mohamed Ben Abdellah University, Fez, Morocco
[2] Functional Ecology and Environment Engineering Laboratory, Faculty of Sciences and Techniques, University of Sidi Mohammed Ben Abdellah, Fez, 30000, Morocco

Abstract. The Temsamane massif is part of the external Rif of Morocco and is distinguished by more intense deformations, linked to its topographical, lithological and structural characteristics. Many natural hazard phenomena, and therefore damage and loss of resources and people, are present. The detailed work on these activities remains much localized using traditional techniques. The analysis using differential interferometry techniques of Synthetic Aperture Radar (SAR) images (DINSAR) made it possible to determine the instability and vulnerability to subsidence risks from two images from the Sentinel satellite of two different years (2018 and 2022). The results obtained show the presence of some areas of subsidence in the urban sector, the continuation of shrinkage and slight uplift in the relief areas, and generally instability in rural areas.

Keywords. Radar Interferometry, DINSAR; Subsidence; Uprising; Temsamane; External Rif; Morocco.

1. Introduction

Previous studies of the Rifian domain in Morocco show that the major Nekor fault is made up of several sections evolving independently in time and space. The Temsamane massif is located in a corner which generates more intense deformations, thus the structural, stratigraphic, tectonic and metamorphic correlations, carried out recently in the outer Rif, show the fragility and instability of this massif which are manifested by networks recent flaws. In addition, the lithological characteristics of the massif favor these phenomena through the existence of shales, sandstones, sands, marls and clays. Thus, the Rif region in Morocco still experiences natural hazards such as earthquakes, floods, landslides, etc. as demonstrated by [1]. This is why the government is launching numerous works, studies and monitoring to prevent these disasters and put forward effective interventions by limiting the damage and preserving human security and the resources necessary for Morocco's prospects for sustainable development. Among the favored studies, those to map risks of different natures, in particular the modeling of floods, areas vulnerable to fires, etc. as demonstrated [23]. For all these reasons, the Temsamane area was chosen to apply the technique of radar interferometry to the mapping of areas vulnerable to subsidence, exploiting this recent technique for geological studies in this area with free data and tools necessary also available and offered by the European Space Agency [2, 3].

2. Geology of the study area

The Temsamane massif includes Paleozoic and Mesozoic terrains with superimposed structures and polyphase ductile deformation, characteristics of WSW-ENE movement [4 – 6]. The area undergoes MP-BT metamorphism. This massif includes the deepest units of the outer rift. The deformations are

* Corresponding author: mourjanemohammed@gmail.com

relatively intense because they are stuck between the Nekor fault and the discordant fault north of Gareb. The Temsamane massif peaks around 1000 m above sea level and is oriented approximately E-W. It is bounded on the south side by a system of normal faults oriented N060, collapsing the Kert basin to the south. The non-conforming terrain consists of detrital conglomerates alternating with sandstone, sand, shale, clay and marl.

3. Materials and methods

This study was carried out using radar images from the S1A and S1B mission sentinel platform with the IW acquisition mode, and SLC product type on a descending trajectory for S1A and an ascending trajectory for S1B. These images are characterized by the amplitude which provides information on the energy backscattered in the direction of the sensor and which depends on several characteristics of the target such as roughness and absorption and the phase which is a measure of distance between the radar sensor and the target. The structure of the target and its dielectric properties cause phase rotation. Sending and receiving polarimetric VV (vertical-vertical) radiation [7- 10].

The sag measurement is based on the Dinsar SAR differential interferometry process by exploiting the data contained in the signal phase of input images of the same target, taken on different dates, two images for each calculates a master image and the other slave, forming the so-called differential interferogram by subtracting the topographic contributions from the interferometric phase with a DEM (Digital Elevation Model) reference, which makes it possible to find the phase component linked to the movement. Table 1 shows the input data.

Table 1. Input data for the construction of interferograms.

Interfero-gram	Master image	Slave image	DEM
1	S1B : 2018-02-10	S1B: 2018-05-17	SRTM 1sec HGT
2	S1A : 26-01-2022	S1A : 13-07-2022	SRTM 1sec HGT

Differential interferometry of SAR images (DINSAR) is performed using a set of methods with at least two complex radar images in order to obtain additional information about the objects present in a single radar image. The calculation of the interferogram is done, pixel by pixel, from the phase difference of the two radar images acquired at two different dates, in close shooting described in the following equation:

$$\Delta\phi = \Delta\phi d + \Delta\phi a + \Delta\phi t + \Delta\phi dc + \Delta\phi r + 2k\pi$$

Where:

$\Delta\phi$ *mean phase difference*

$\Delta\phi d$*: phase difference related to possible ground displacement, measured along the line of sight.*

$\Delta\phi a$*: phase difference due to changing atmospheric conditions between image acquisitions.*

$\Delta\phi t$*: phase difference related to the topography of the site.*

$\Delta\phi dc$*: phase difference from geometric and temporal decorrelations (generated by surface condition variations, and by image acquisition variations).*

$\Delta\phi r$ *: residual phase difference (noise) resulting from processing (registration, SAR).*

The processing carried out with SNAP software with the steps explained in Figure 1. The treatments remove all the effects influencing the phase difference and only retain the difference depending on the displacement of the ground. SNAP is free software downloadable from the European Space Agency ESA website and is distributed under the GNU license, developed and supported by ESA [10]. The software provides an efficient tool for processing optical and radar satellite data.

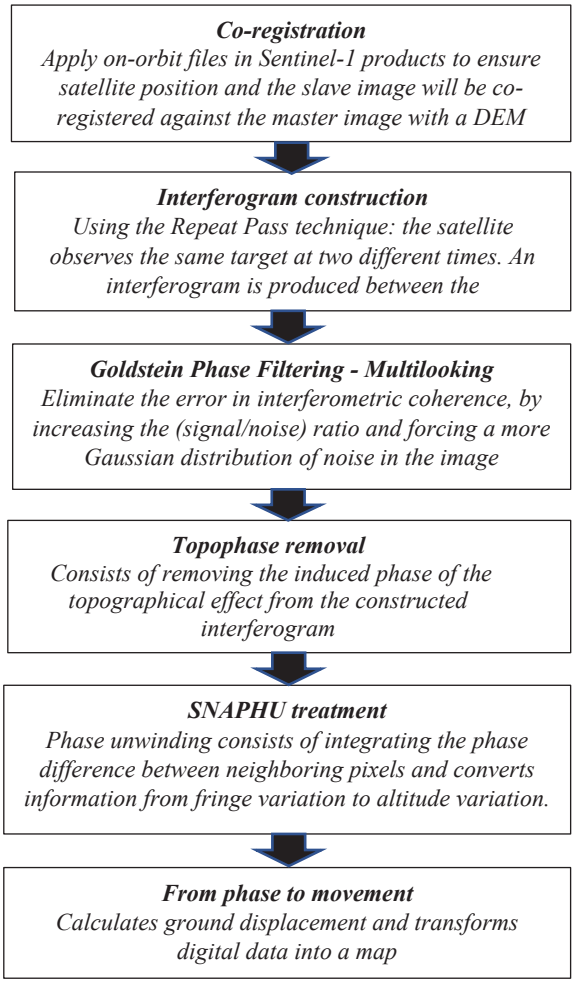

Fig. 1. The steps of processing data on SNAP Software

Thus, to offer an effective tool for processing satellite data from optical and radar images, it is important to download external plugins or activate them, for example sen2cor for Sentinel-2 necessary for level 2, and SNAPHU for DINSAR analysis of Sentinel1 images. Figure 1 illustrates an explanatory diagram of the processing steps.

4. Results and discussion

After applying the files of four radar images of input data into orbit, we ensured the satellite position and precise velocity information, and made two interferograms between the interferometric couple (master and slave), knowing that the coherence image estimate of the recomputed complex image stack is included. Figure 2-a shows an example of an interferogram for the year 2022. Several detonations can be distinguished: each interferometric fringe represents a complete cycle of 2π and therefore half the wavelength of the sensor (λ = 5.66 cm). Figure 2-b represents the coherence map of the same interferogram. The two images are almost consistent with each other in several areas, which indicates good processing.

The result of the processing and calculation is shown in Figure 3, for the Temsamane region; (a) the movement of the ground between 02/10/2018 and 05/17/2018 and (b) between 01/26/2022 and 07/13/2022. We manipulated the color palettes of the map that the SNAP software gives by default, to diversify the visualization and better extract the interpretations. Another region appears important to the southeast of the study area, this is the case of Douar Ouchanen. The raw displacement map is in (e) while the manipulation map is present in Figure 4.

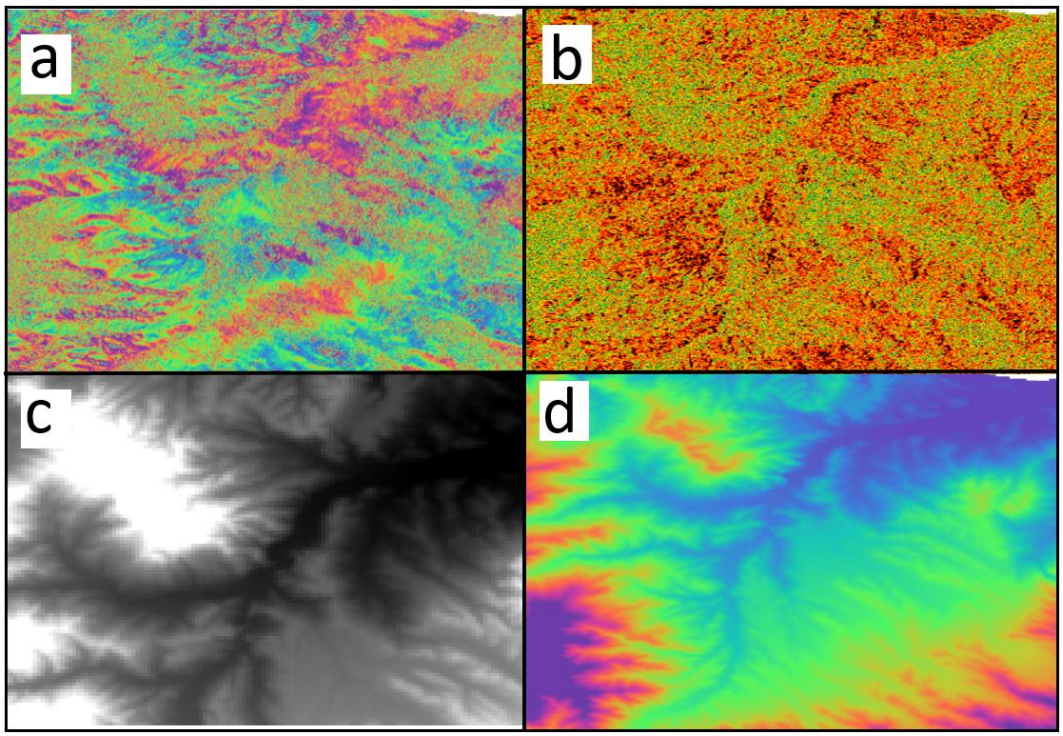

Fig 2. Example of an interferogram (2022); a: phase, b: coherence of two images: c: DEM (SRTM), d: Topophase removal

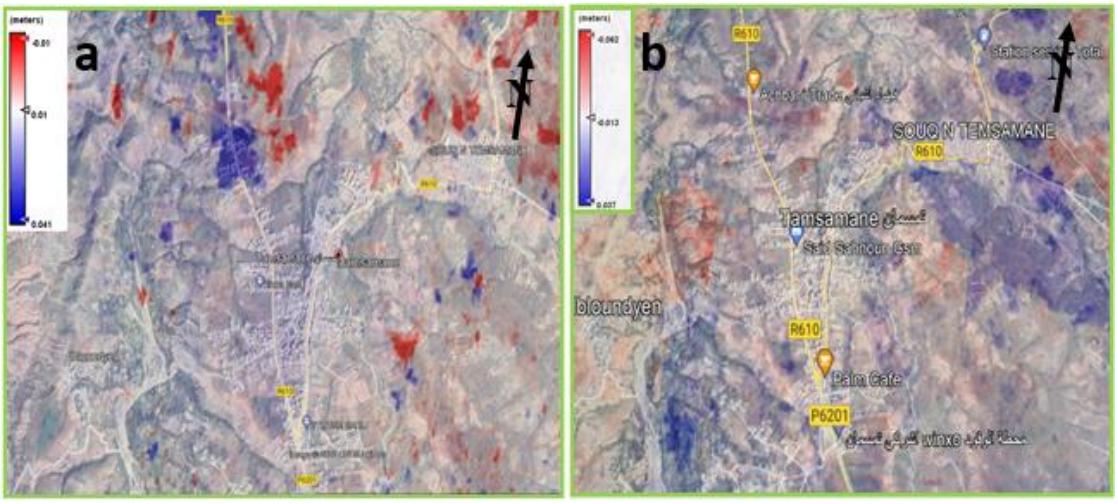

Fig. 3. Same displacement map of the Temsamane region with different color palette; a (2018), b (2022)

We see that there are regions with negative values and others with positive values. The former reflects the phenomenon of subsidence and the latter reflect the phenomenon of uplift. The objective of our study is to focus on subsidence regions, and to monitor the variability between the year 2018 and the year 2022. For the Temsamane region, we observed, for the year 2018, that generally the urban area, where constructions and buildings are located, remains almost calm, while there is little subsidence (on the centimeter scale) in certain rural areas. However, in 2022, we can see the appearance of subsidence in certain urban areas (Figure 5). Three large areas surrounded by the red circle in the center of Temsamane containing residential or service buildings, roads and streets, and undeveloped land.

The village of Ouchanen did not experience any change in its population during the study period from 2018 to 2022. The vegetative zones which continue to decrease are mainly located to the north of the village. The Beni Milikchen area near the mosque shows continuous surface movement with weak uplift, alongside another of weak retreat in two maps from 2018 and 2022 (Figure 6). This instability of the terrain can be linked to tectonics with the presence of the Nekor fault and that to the north of Gareb and the lithological nature of the facies with detrital conglomerates alternating with less stable and more mobile sandstones, sands and marls. Anthropogenic participation can be ignored due to the large areas concerned (several hectares). Table 2 summarizes the results of the study of the three sectors studied.

Table 2. Results of the study of three major subsidence zones

Area	***Period***			
	2018		***2022***	
	Urbane	***Rural***	***Urbane***	***Rural***
Tamsa-mane	*Almost stable*	*Subsidence to the EAST (maximum ≈ -3.10^{-3} m)*	*Three subsidents area (≈-2,1.10^{-2} ; - 3.10^{-2}m)*	*Many subsidents areas (≈ -2,1.10^{-2} m ; -3.10^{-2}m)*
Ouchan-en	*Almost stable*	*Several subsidence areas (maximum ≈ -3.10^{-3} m)*	*Almost stable*	*Subdudence especialy in the north (≈ -1,4.10^{-2} ; - 3.10^{-2}m)*
Beni Milikch-en	*Uplift ≈ 4,1.10^{-2}m & subsidence ≈ -1.10^{-2}m*	----------	*Uplift (≈ +1,7 .10^{-2}m) & subsidence ≈ -4.10^{-2}m)*	----------

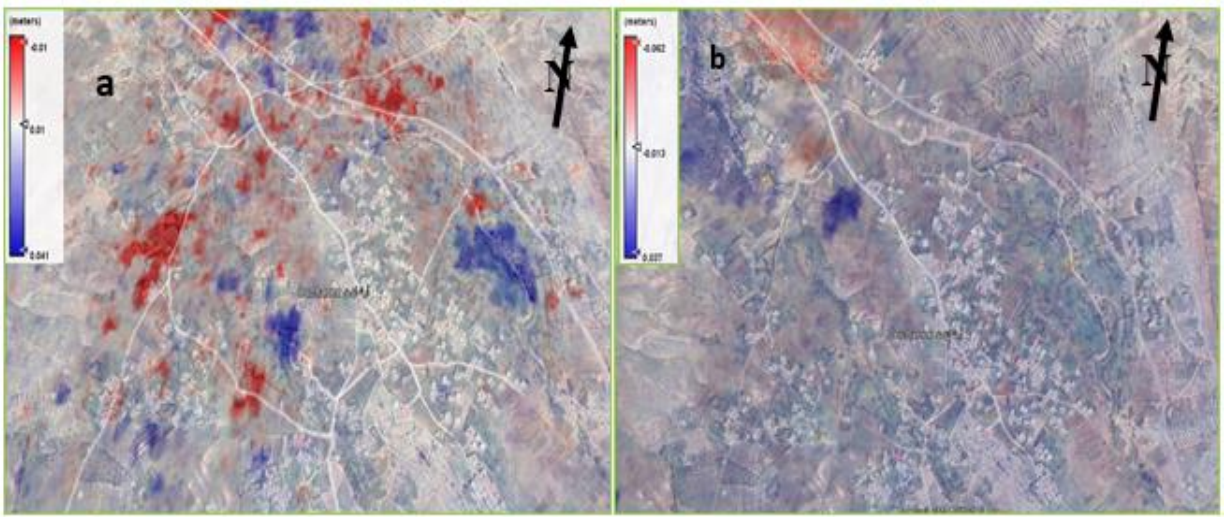

Fig. 4. Displacement map of the Ouchanen region with different color palette; a (2018), b (2022)

Fig. 5. Urban areas affected by soil shrinkage in 2022, Temsamane region

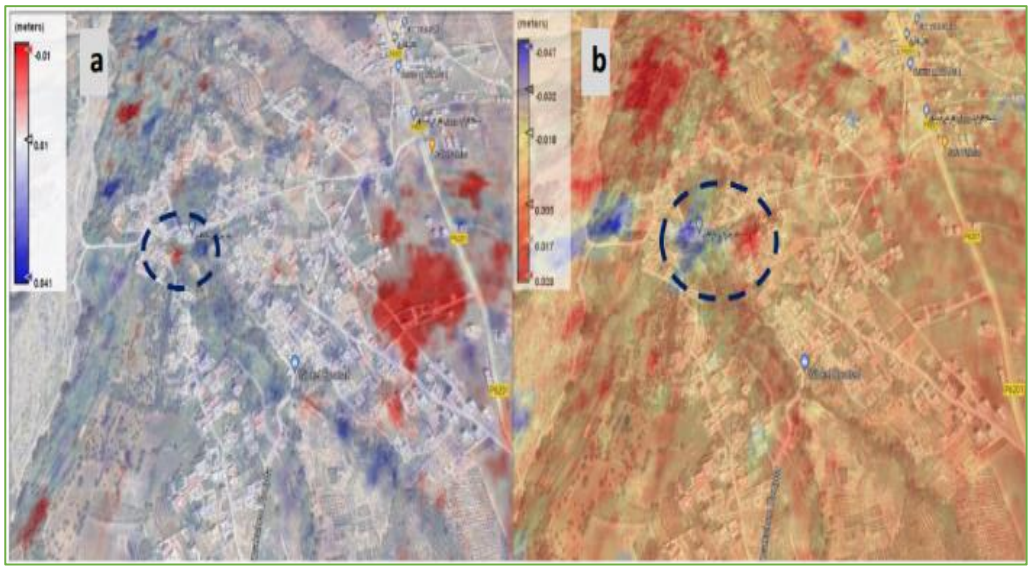

Fig. 6. Soil displacement in the Beni Milikchen region; (a): between 10-02-2018 and 17-05-2018, and (b): between 26-01-2022 and 13-07-2022

5. Conclusion and perspective

The differential radar interferometry (DINSAR) method made it possible to measure the relative movements of the ground surface from two radar images acquired on different dates. For the period from 2018 to 2022 alone, this method revealed the zones of subsidence and uplift with centimeter-scale precision. It thus presents strong potential for the study of natural risk, particularly in this part of the External Rif known for its tectonic and seismic activities. We were thus able to show subsidence movements in the urban and especially rural areas, thanks to a careful selection of radar images in a very close geometry (a baseline less than 50m). The lack of spatial coherence in vegetated areas in rural areas limited the highlighting of small-scale movements and only movements that were sufficiently extensive, linear and continuous over time were represented in form on the phase difference images between both dates.

Acknowledgments: The authors thank the European Space Agency for radar data and software and also the reviewers for their suggestions to improve the quality of this paper. This research is carried out with the assistance of the Hassan II Academy of Sciences and Technology, Rabat (Morocco).

References

1 V. Pascazio, G. Schirinzi, *Multifrequency InSAR height reconstruction through maximum likelihood estimation of local planes parameters*, IEEE Transactions on Image Processing, **11**, 12, 1478-1489 (2002).

2 F. Kugler, D. Schulze, I. Hajnsek, H. Pretzsch, K. P. Papathanassiou, *TanDEM-X Pol-InSAR Performance for Forest Height Estimation*, IEEE TG&RS, **52**, 10, 6404-6422 (2014).

3 J. Li, W. Wang, G. Chen, Z. Han, *Spatiotemporal assessment of landslide susceptibility in Southern Sichuan, China using SA-DBN, PSO-DBN and SSA-DBN models compared with DBN model*, ASR, **69**, 8, 3071-3087 (2022).

4 L. Asebriy, J. Bourgois, T. E. Cherkaoui, A. Azdimousa, *Evolution tectonique récente de la zone de faille du Nékor: importance paléogéographique et structurale dans le Rif externe, Maroc,* JAE SME, **17**, 1, 65-74 (1993).

5 Y. Hervouet, P. de Luca, *Place de l'unité chaotique de Gareb - Kebdana dans l'orogénie rifain ; implications géodynamiques*, B SGF, **S7-XXII**, 3, 305-310 (1980).

6 H. Haddoumi, A. Charrière, B. Andreu, P.O. Mojon, *Les dépôts continentaux du Jurassique moyen au Crétacé inférieur dans le Haut Atlas oriental (Maroc) : paléoenvironnements successifs et signification paléogéographique*, C G, **CG2008**, A06, **1**, (2008).

7 D. P. S. Bekaert, A. Hooper, T. J. Wright, *A spatially variable power law tropospheric correction technique for InSAR data*, J GRSE, **120**, 2, 1345-1356 (2015).

8 G. Ferraiuolo, V. Pascazio, G. Schirinzi, *Maximum a posteriori estimation of height profiles in InSAR imaging*, IEEE Geoscience and Remote Sensing Letters, **1**, 2, 66-70 (2004).

9 S. K. Ebmeier, J. Biggs, T. A. Mather, J. R. Elliott,

G. Wadge, F. Amelung, *Measuring large topographic change with InSAR: Lava thicknesses, extrusion rate and subsidence rate at Santiaguito volcano, Guatemala*, EPS L,**335-336**, 216-225, (2012).

10 D. Massonnet, K. L. Feigl, *Radar interferometry and its application to changes in the Earth's surface*, RG, **36**, 4, 441-500 (1998).